Postmortem assessment of the WEST Fiber Bragg grating and thermocouple diagnostic performances with HADES

J. Gaspar, Y. Corre, Y. Anquetin, J-L. Gardarein, C. Pocheau, H. Roche, N. Vignal, A. Bureau, Romain Cotillard, M. Houry, et al.

▶ **To cite this version:**

J. Gaspar, Y. Corre, Y. Anquetin, J-L. Gardarein, C. Pocheau, et al.. Postmortem assessment of the WEST Fiber Bragg grating and thermocouple diagnostic performances with HADES. Fusion Engineering and Design, 2023, 190, pp.113525. 10.1016/j.fusengdes.2023.113525 . cea-04087261

HAL Id: cea-04087261

https://cea.hal.science/cea-04087261v1

Submitted on 13 Jun 2023

HAL is a multi-disciplinary open access archive for the deposit and dissemination of scientific research documents, whether they are published or not. The documents may come from teaching and research institutions in France or abroad, or from public or private research centers.

L'archive ouverte pluridisciplinaire **HAL**, est destinée au dépôt et à la diffusion de documents scientifiques de niveau recherche, publiés ou non, émanant des établissements d'enseignement et de recherche français ou étrangers, des laboratoires publics ou privés.

Post-mortem assessment of the WEST Fiber Bragg grating and thermocouple diagnostic performances with HADES

J. Gaspar[a], Y. Corre[b], Y. Anquetin[a], J-L. Gardarein[a], C. Pocheau[b], H. Roche[b], N. Vignal[b], A. Bureau[b], R. Cotillard[c], M. Houry[b], G. Laffont[c], T. Loarer[b], M. Missirlian[b], P. Reilhac[b], E. Tsitrone[b] and the WEST team[d]

[a]*Aix Marseille Univ, CNRS, IUSTI, Marseille, France*
[b]*CEA Cadarache, IRFM, F-13108 St Paul lez Durance, France*
[c]*CEA, LIST, Gif-sur-Yvette Cedex 91191, France*
[d] *See http://west.cea.fr/WESTteam*
Corresponding author email address: jonathan.gaspar@univ-amu.fr

Abstract. Plasma facing components temperature measurement is required to ensure safe high power for long pulse tokamak operation and for physics studies. During the WEST phase 1, a set of 20 thermocouples (TC) and 4 fibers Bragg grating (FBG) have been exposed to five experimental campaigns with 3889 plasmas for a total plasma duration of about 7h15 and 21.2 GJ of cumulated injected energy. This paper presents the performances in terms of response time and high temperature sustaining assess with high heat flux tests performed in the HADES facility. The response time of the TC remains at the same level as before their installation in the divertor. However, the FBG have shown clear increase of their response time depending on the location due to a degradation of the thermal contact of the graphite adhesive and the FBG or component. Finally, one regenerated FBG has been exposed to high temperature, showing that absolute temperature measurement is found reliable up to 1100°C with the start of some spectrum degradations. Full erasure of the grating is obtained after 10s at 1200°C well above the stable temperature of 900°C of the regenerated FBG.

1. Introduction

One of the main goals of WEST is the assessment of power handling capabilities and lifetime of tungsten divertor components under high heat flux and high fluence operation in a full W tokamak environment [1]. During the first five experimental campaigns (named C1 to C5), WEST operated with a mix of actively cooled ITER like tungsten plasma facing units (PFUs) and inertial tungsten coated graphite components [2]. The preliminary step towards testing the tungsten ITER like components under ITER relevant heat flux (10 MW/m² in steady state), is to characterize the heat flux deposition pattern in terms of intensity and decay length. For this purpose, a set of complementary diagnostics allowed characterizing properties of the heat loads on the lower divertor: arrays of embedded thermocouples (TC) [3] and Fiber Bragg Gratings (FBG) sensors [4], infra-red thermography (IR) [5] and arrays of flush-mounted Langmuir probes (LP) [6]. Among these diagnostics the TC and FBG diagnostics allowed to study and built a heat flux database during the first phase of WEST: from the the first ohmic diverted plasma [7] up to the high power (up to 8 MW total injected power during 4 s) and high energy (up to 90 MJ total injected energy in lower single null configuration) steady state L-mode plasma experiments were performed in the last experimental campaigns [8]. As WEST entering in his phase 2 with a full ITER-like divertor [9], the TC and FBG embedded in W-coated graphite PFU have been removed from the machine and available for post-mortem study to evaluate their performances.

During the last campaign some sensors have shown a degradation in dynamic during heating and cooling phases of the components with an increase of their response time. High heat flux tests have been performed using the HADES (High heAt loaD tESt) electron beam facility [10] to evaluate the dynamic and temperature performances on a wide range of heat flux and shot duration. The lower divertor and its exposure during the WEST phase 1 is presented in section2. Section 3 presents the HADES electron beam facility. Section 4 presents the response time performances of each diagnostic assessed in HADES.

Finally, last section studies the temperature measurement capability of the regenerated FBG at high temperature up to 1200°C well above the design temperature of 900°C.

2. WEST lower divertor during the WEST phase 1

The phase 1 of operation of WEST extending from 2017 to 2020 is composed of five experimental campaigns named from C1 to C5 [2]. During this phase, the lower divertor was composed of a mix of actively cooled ITER-like and inertially cooled W-coated graphite PFUs. For the second phase of operation starting in 2022, the lower divertor is fully equipped with ITER-like PFUs with ITER relevant shaping, allowing plasma operation with long and high-energy pulses [9]. During the WEST phase 1, 3889 plasmas have been performed for a total plasma duration of about 7h15 and 21.2 GJ of cumulated injected energy (see table 1), mainly electron heating using lower hybrid launchers (LHCD heating), in lower single null (LSN) or upper single null (USN) configuration. During this period 2580 pulses ended with a disruption leading to damages on the ITER-like PFU [11].

	Nb Plasma	Ip max (kA)	Duration max (s)	Cumul (s)	Disrup-tions	Disrup-tivity	LH (pulse)	LH max (MW)	W LH total (MJ)	IC (pulse)	IC max (MW)	W IC total (MJ)	Boro
C2 Nov17-Feb18	716	805	10.5	1553	744	76%	168	2.5	95.5	0	0	0	0
C3 July-Dec18	1076	818	37.5	7329	796	74%	572	5.3	4947	186	1.4	105	3
C4 – D2 July-Nov19	1112	1004	55	9678	763	69%	509	5.4	7823	339	5.7	1139	13
C4 - He Oct-Nov19	330	709	30	2991	279	85%	196	4.5	4300	21	0.3	3	0
C5 Nov20-Jan21	655	806	23	4630	460	70%	280	5.4	2625	145	3.7	182	2

Table 1. Plasma exposure during WEST phase 1. C1 is not described as no sustained plasma has been obtained in this campaign. Nb plasma: number of plasmas with Ip>100kA performed in each campaign. Ip max: maximum plasma current performed in the campaign. Duration max: maximal during of a single pulse during the campaign. Cumul: Cumulative time of the plasma during each campaign. Disruptions: number of plasma ended with a disruption. LH: Low Hybrid heating. IC: Ion cyclotron heating. Boro: number of boronization performed in the campaign.

In LSN configuration the inner strike point and outer strike point are located on the lower divertor (see figure 1 a) which is composed by 12 independent toroidal sectors of 30°. Each sector is equipped by 38 plasma facing units, thus a total of 456 PFUs is required to cover the full divertor ring (see figure 1 b). The W-coated graphite is divided in two separate components, one in the Low Field Side (LFS/outer) and one in the High Field Side (HFS/inner). The WEST lower divertor is monitored by a set of complementary diagnostics allowing the characterization of the heat load properties: 20 embedded TCs located at 7.5mm below the surface [3], 4 FBGs [12] embedded at 3.5 and 7mm below the surface (see figures 1 c and d). The TC are embedded in a lateral hole of 1cm with graphite adhesive and the FBG are embedded in a lateral groove of 4mm with also graphite adhesive (see figure 1d). The diagnostics are spread over the 12 divertor sectors keeping symmetric toroidal location of the sensors regarding the magnetic field toroidal modulation (ripple effect). Diagnostics have been working successfully from the first plasma breakdown achieved in WEST up to the dismantling of the uncooled divertor done four years later. The operation of these diagnostics allowed to observe the increase of the deposited heat flux on the outer strike point region over the campaigns up to 6 MW/m² [8] and monitor temperature up to 830°C [13]. They also allow to study of the emissivity evolution of the PFU by monitoring the PFU temperature between pulses [14].

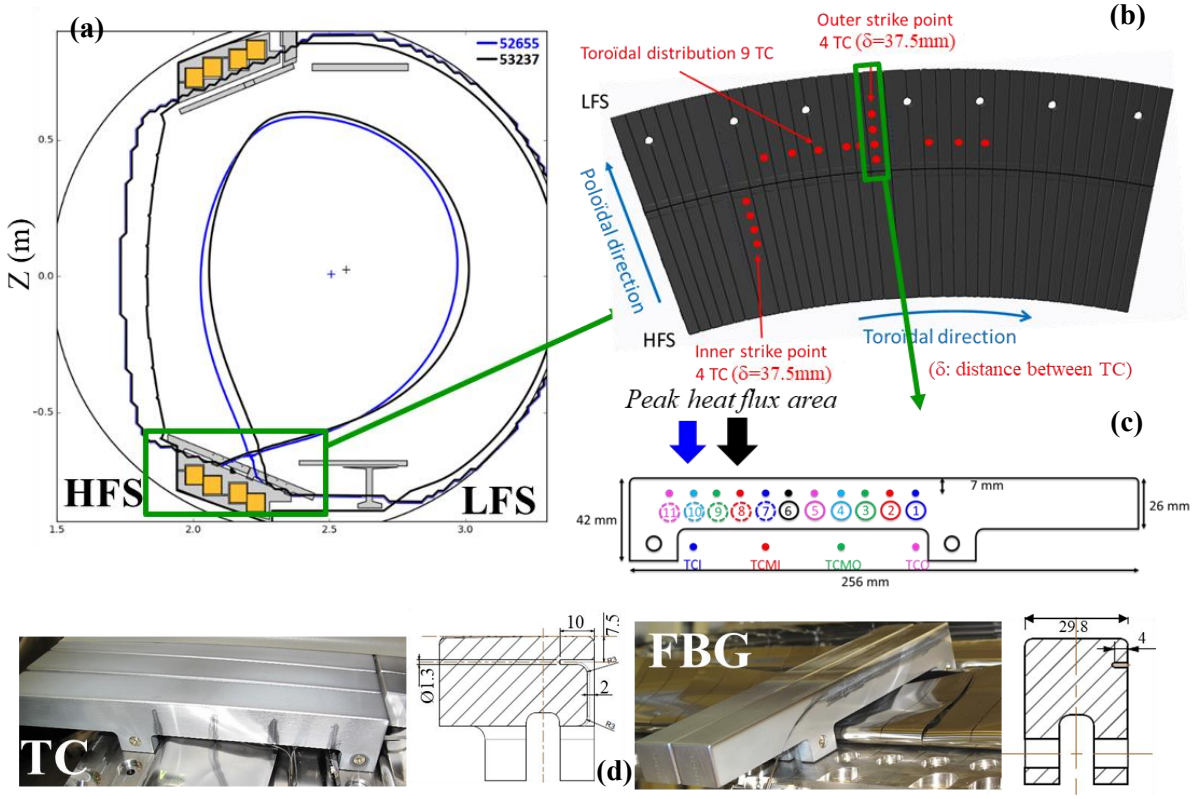

Figure 1. (a) Poloidal magnetic field configuration for two magnetic configurations in the WEST Tokamak. (b) Lower divertor view of the instrumented sector with the 16 TC installed. (c) 2D poloidal cross section of the PFU with FBG locations and corresponding poloidal TC locations below (the surface exposed to the plasma is on the top). (d) Pictures of the instrumented PFU with TC and FBG and 2D toroidal cross section.

3. HADES facility

HADES (High heAt loaD tESt) is an electron beam facility built at CEA-IRFM [10]. The aim of this facility is to test the PFU and to assess to their heat exhaust capabilities facing high heat fluxes. The facility can cover thermal fatigue tests, critical heat fluxes and thermal shocks. To do so, the HADES electron beam gun permits to simulate steady state experiments with thermal flux up to a few tens MW/m² and transient events with thermal energy up to 1 GW/m² during a few milliseconds. A programmable sweep system allows several kinds of power repartition (uniform and peaked). The maximum gun power is 150kW in continuous mode. The beam diameter is about 12mm, with a Gaussian shape. The power is deposited on the target by a programmable sweep system scanning a pattern and a large set of various depositions is possible: line, spiral, patterns is available raster, cycloid, mesh, etc. For this study, we used a mesh pattern, which gives uniform heat flux over the specified area (red rectangle in the figure 2b). The facility includes a large volume vacuum vessel (8m^3) suitable for instrumented mock-up up to 2 m long, with dedicated windows for optical observations and surface temperature measurement diagnostics (IR camera (25-1500°C) see figure 2b, pyrometers (<2700°C)). A pumping group ensures a vacuum pressure of 10^{-3} Pa inside the vessel. The HADES facility is equipped with a pressurized water-cooling loop (3.5 MPa, 50 to 220 °C, 6 kg/s) allowing studies of

actively water cooling PFUs. Here only the copper shield is water cooled as the studied PFU are inertial PFU without water cooling channel in the component.

For this study three outer PFUs have been tested in HADES, the Q6A PFU#23 with 1 TC, the Q3A PFU#21 with 1 FBG and the Q4A PFU#21 with 1 FBG. All the PFUs were at symmetric toroidal location leading to equivalent heat loads during their exposure in WEST. Two kinds of study have been performed in HADES. The first one is to evaluate the response time of all sensors using heat flux of about 1MW/m² during few seconds. The second study is to evaluate the behavior of the regenerated FBG with heat flux about 2MW/m² during tens of seconds to reach high temperature, typically above 900°C, when the erasure of the gratings is expected. Figure 2 a) shows one of the PFU mounted for HADES test and the figure 2b shows an IR image of the PFU during the response time tests. Despite the uniform heat flux applied on the PFU the blackbody temperature measured with the IR system is not uniform. This is due to the high emissivity variation on the PFU due to the Tokamak exposure [15]. In this area the emissivity varies about a factor 5 explaining the factor 2 observed in the blackbody temperature.

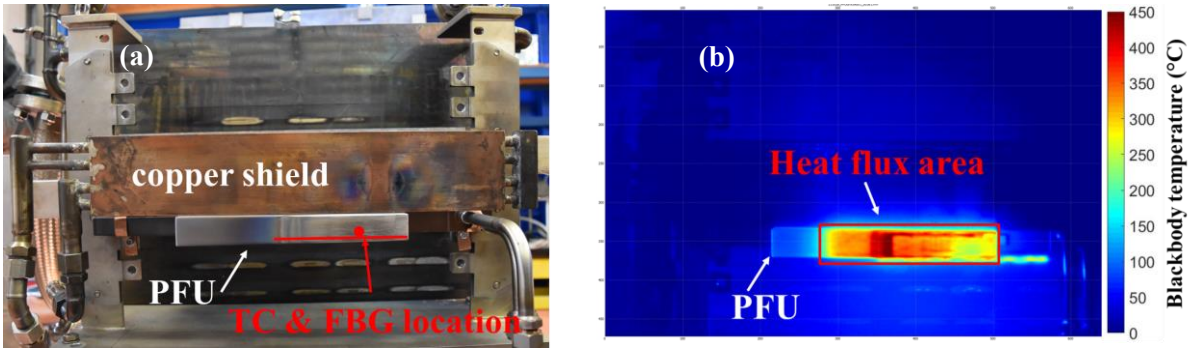

Figure 2. (a) Picture of one PFU mounted in HADES. (b) IR image during the heating of the PFU.

4. TC & FBG response time study

When a thermal sensor (TC or FBG) is submitted to a fast temperature change, it takes some time to reach the true temperature. This sensor response time τ can be characterized through a simple first order equation giving its step response u(t) defined by:

$$u(t) = \left(1 - e^{-\frac{t}{\tau}}\right) \quad (1)$$

where τ is the response time defined as the duration required for the sensor to exhibit a 63% change from an external temperature step [16]. The response times of the TC and FBG have been evaluated to be about 0.25s before their installation in WEST [7]. This response time include the response time of the sensor itself and the response time of the graphite adhesive used to have a good mechanical and thermal contact.

4.1. TC

Figure 3 a) shows the time evolution of the uniform heat flux deposited on the outer PFU#23 with 1 TC. The measured temperature during this shot is plotted in black in the figure 3 b). The blue curve corresponds to the temperature calculated with the finite element method software CAST3M [17]. The TC response time is estimated by a non-linear least square algorithm, minimizing the discrepancy between the measured temperature and the calculated temperature convoluted with the step response u(t) by adjusting the value of τ. The best match is shown with a red dotted line in the figure 3 b) with τ = 0.295 ±0.01s. A total of 5 shots have been performed to evaluate the response time, an average value

of τ = 0.28 ± 0.02s has been found showing the reproducibility of the estimation. The response time value is equivalent to the 0.25s evaluated before the PFU installation showing no degradation of the TC performance after the WEST phase 1 exposure. To extend this observation to the other TCs not studied in HADES, their time behaviours have been compared to the TC studied here during the last pulse of last experimental campaign. As all the TC exhibit equivalent time behavior during the heating and cooling phase of this very last pulse, one can conclude that the TC diagnostics has no degradation after the WEST phase 1.

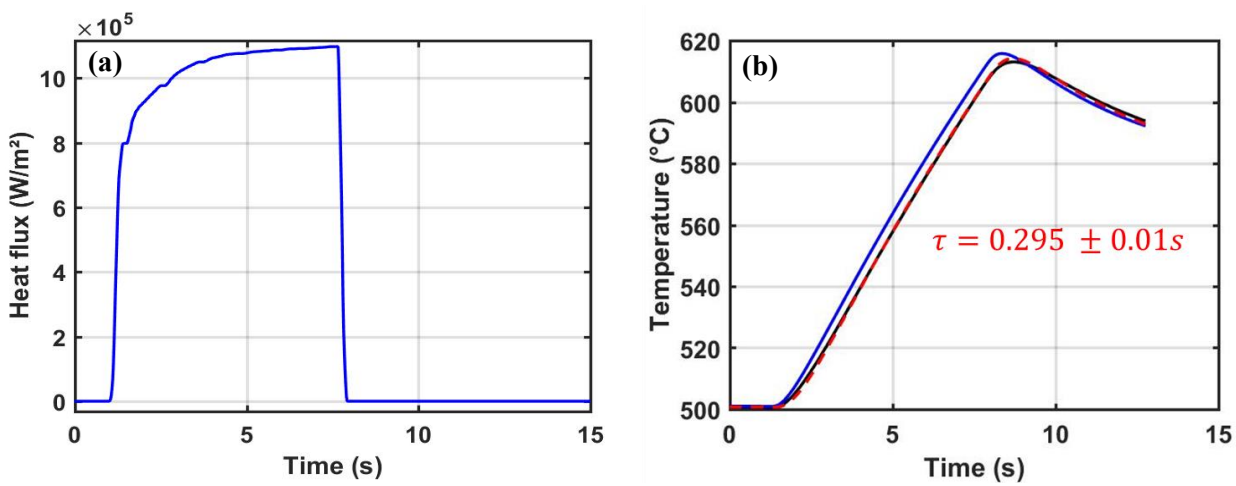

Figure 3. (a) Heat flux deposited on the PFU Q6A with TC. (b) (black) TC measurement (blue) CAST3M calculation with the deposited heat flux without response time (red, dotted line) CAST3M calculation convoluted with equation (1) and response time of τ=0.295s.

4.2. FBG

Two PFUs with FBG have been tested with a total of 50 shots with different initial temperature from 100 to 350°C. This different initial temperature can be obtained thanks to the inertial behavior of the PFU which is not water cooled.

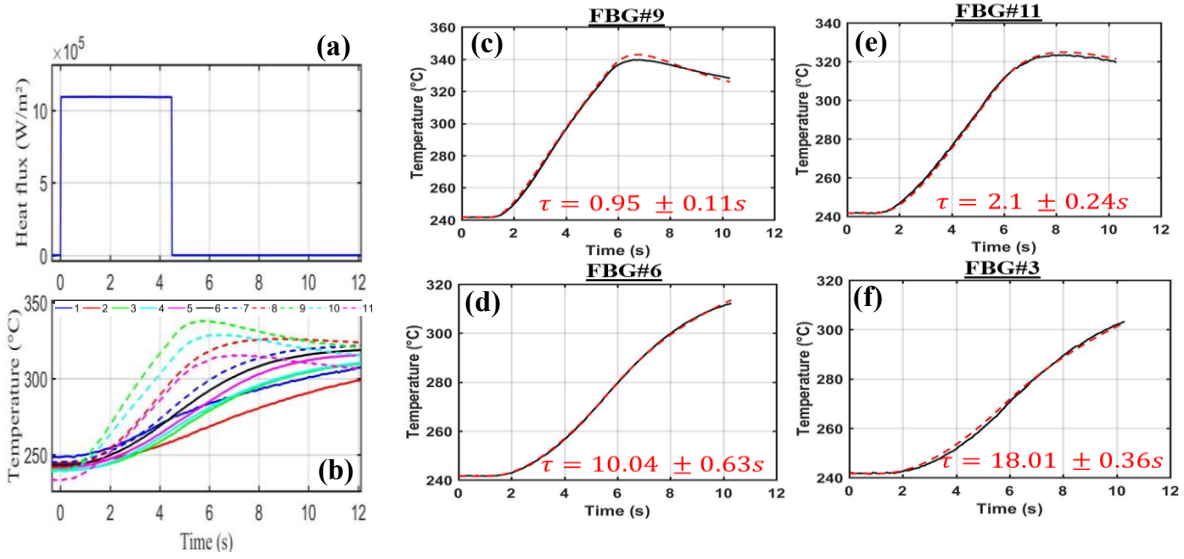

Figure 4. (a) Heat flux deposited on the PFU#21 Q3A with FBG. (b) Q3A FBG measurement. (c-f) (black) FBG measurements of the gratings 9/11/6/3 (red, dotted line) CAST3M calculation convoluted with equation (1) and estimated response time τ at fixed initial temperature of 240°C.

Figure 4 a) shows a typical heat flux time evolution used for the estimation, with about 1.1 MW/m² during 4.5s. The resulting temperature measured by the FBG in the PFU#21 Q3A is plotted in the figure 4b). Despite the uniform heat flux the gratings exhibit important differences in their time behavior showing different response time for each grating. Figures 4 c) to f) illustrate the range of response time estimated for this shot with value from $\tau = 0.95 \pm 0.11$s to $\tau = 18.01 \pm 0.36$s, corresponding to an increase of the response time from the nominal value (0.25s) about a factor 4 and 72, respectively. The estimated values of τ are summarized in the table 2 and plotted in the figure 5 a). The smallest response times are for the gratings 8 to 11 which correspond to the high heat flux location in the WEST lower divertor. On the contrary, for the FBG embedded in the PFU#21 Q4A the highest response times are in high heat flux area of WEST as shown in the figure 5 b) and in the table 2. This illustrates that the degradation of the FBG response time can not be directly linked to the heat load area during the WEST exposure. This degradation is due to a loss of thermal contact between the sensor and the component due to a degradation of the graphite adhesive used in the groove where the FBG are embedded.

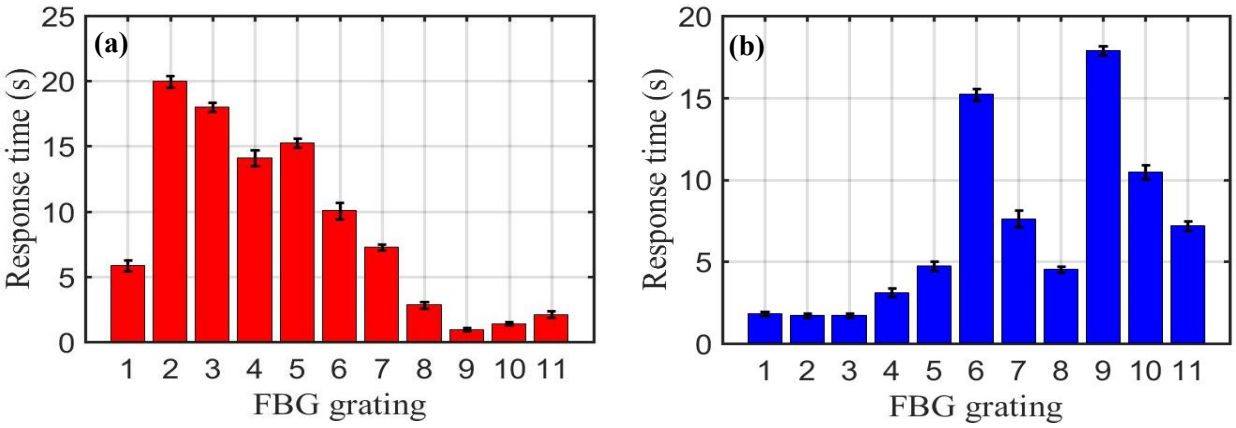

Figure 5. Estimated response time for each grating for the PFU at T_{init}=250°C. (a) Q3A. (b) Q4A.

PFU	FBG1	FBG2	FBG3	FBG4	FBG5	FBG6	FBG7	FBG8	FBG9	FBG10	FBG11
Q3A	5,86	19,95	18,01	14,11	15,26	10,04	7,25	2,82	0,95	1,40	2,10
Q4A	1,84	1,71	1,72	3,11	4,72	15,21	7,61	4,52	17,89	10,47	7,19

Table 2. Estimated response time [s] for each grating for the PFU at T_{init}=250°C. (a) Q3A. (b) Q4A.

It has to be noted that the FBG embedded in the PFU#21 Q3A shows an evolution of the response time for the different grating depending on the initial temperature of the PFU before the shots. Figure 6 shows this dependency with a clear decrease of the response time with the increase of the PFU temperature. This decrease is about a factor 2 for most of the gratings, leading to smaller value for the gratings 8 to 11 down to about 0.4s for the grating #9 compatible with good measurement of the temperature. The other FBG embedded in the PFU#21 Q4A does not exhibit temperature dependency, equivalent response times have been evaluated over the whole range of temperature.

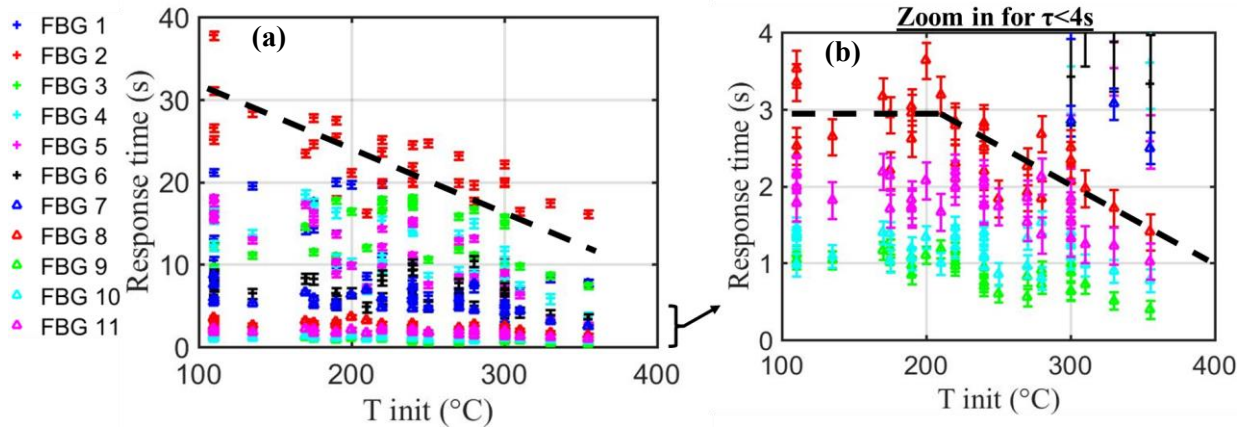

Figure 6. (a) Estimated response time for each grating for the PFU#21 Q3A function of the initial temperature (T_{init}) during the heating. (b) Zoom in for τ<4s.

5. High temperature sustaining of the regenerated FBG

The FBGs are temperature transducer based on a diffraction gratings photowritten by laser into the core of an optical fiber. The FBGs are monitored in reflection by a spectrometer (spectral range of 85 nm between 1510 and 1595 nm), the measured spectrum is composed of 11 peaks at different wavelength depending on the grating (see figure 8). These peaks are narrow spectral bands of the incident light within the fiber reflected by successive, coherent scattering from the index variations of each grating [18]. The principle of the temperature measurement is based on the determination of the wavelength shift of the Bragg peak reflected by the grating. The main limitation is the erasure of the gratings above 400°C. For WEST, regenerated FBG are used as they are high temperature resistant. The regeneration process is to heat up to 920°C the FBG in a furnace. At this temperature the regeneration for all the FBGs is triggering. This method [19] shows that the FBG can survive up to 900°C with long-term use (> 9000 hours). During the WEST exposure the regenerated FBGs have been exposed to temperature up to 830°C without any degradation of the spectrum [13]. The objective here is to investigate the modification of the FBG spectrum for temperature higher than 900°C. HADES is used to heat the PFU#21 Q4A to high temperature with uniform heat flux of 2MW/m². To follow the temperature evolution of the PFU at the FBG location a TC has been added in the groove as the regenerated FBG are calibrated only up to 850°C.

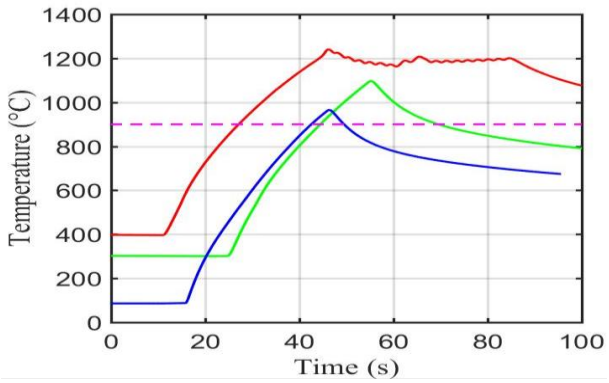

Figure 7. Time evolution of the PFU#21 Q4A at the FBG location measured by TC. (blue) Shot#1 with maximal temperature of 970°C. (green) Shot#2 with maximal temperature of 1100°C. (red) Shot#3 with maximal temperature of 1240°C. (magenta, dotted line) Temperature limit of the regenerated FBG.

Figure 7 shows the temperature evolution of the PFU at the fiber location for the three shots performed in HADES. For the shot#1 the maximal temperature reached is 970°C. After this shot no modification of the spectrum has been observed. During the shot#2 the maximal temperature reached is 1100°C, with a duration of about 20s above the 900°C. After this shot some modifications of the spectrum have been observed. Figure 8 shows the spectrum before (black) and about 300s after (green) the shot when the tile is both at about 300°C. The shot#2 induces an increase of the baseline spectrum which is not impacting the temperature measurement. On the contrary, the Gaussian distribution of the reflected peaks is modified as shown in the figures 8 b) and c) for the grating #2 and 10. These modifications of the Gaussian distribution induces a shift of the maximal Bragg wavelength measured by the system. Finally, these modifications induce acceptable error about 30°C in the temperature measurements.

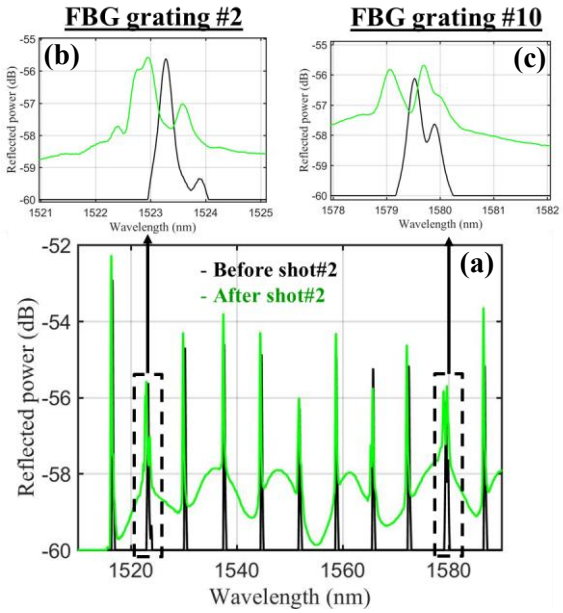

Figure 8. Measured spectrum at 300°C (black) before and (green) after the shot#2. (a) full spectrums. (b) Zoom in for the grating #2. (c) Zoom in for the grating #10.

For the shot#3, the temperature evolution is shown in red in the figure 7. The temperature is about 400°C at the beginning and increase up to 1240°C and finally stabilized at 1200°C during 40s. Figure 9 shows the spectrum measured during the heating from the start (black) until the full erasure of the gratings (red). During the heating the Bragg wavelength of all the gratings shift to higher wavelength values as expected [18]. As observed during the shot#2 the baseline of the spectrum increases from about -58dB to a stable value of -53dB when the temperature of 1200°C is reached (cyan). Then the gratings start to disappear with a full erasure observed after 10s at 1200°C. After the cooling the measured spectrum remains flat without any peak confirming the erasure of the gratings.

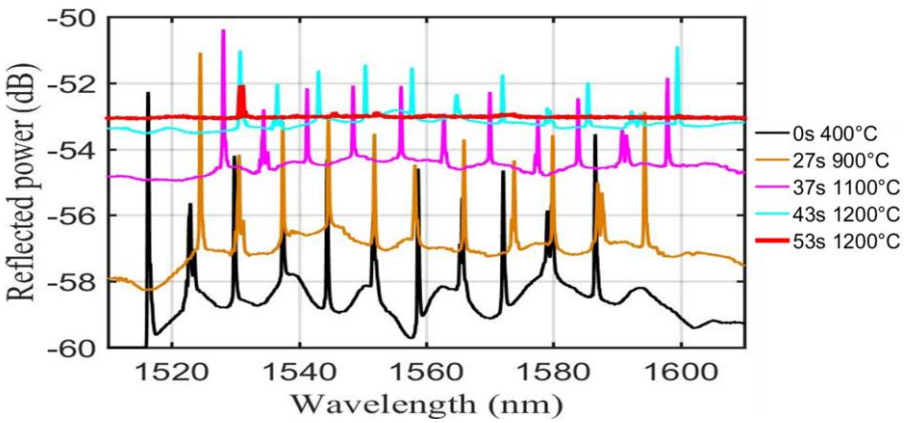

Figure 9. Measured spectrum during the shot#3

6. Conclusion

The performances of the TC and FBG diagnostics have been evaluated after the WEST phase 1 with the HADES facility. During this phase, 3889 plasmas have been performed for a total plasma duration of about 7h15 and 21.2 GJ of cumulated injected energy with a high number of disruptions about 2580. The TC diagnostic has shown an average response time of 0.28s equivalent to the one evaluated before the installation in the machine showing no degradation of the diagnostic dynamic. For the FBG diagnostics, the first degradations of the response time observed during the last experimental campaign have been confirmed with response time from 0.4 to 30s depending on the location and the temperature. This increase of the response time is due to a degradation of the graphite adhesive thermal contact used in the groove where the FBG are embedded and not because of any degradation/erasure of gratings.

One regenerated FBG has been exposed to high temperature showing a good sustaining for temperature above the stable temperature of 900°C for which the fiber has been designed. The first spectrum modification has been observed when the temperature reached 1100°C inducing a baseline increase of the spectrum and a deformation of the Gaussian distribution of the Bragg wavelength of different grating. These deformations induced an error of 30°C. Finally, the full erasure of the grating happened after 10s at 1200°C well above the design temperature.

Acknowledgments

This work has been carried out within the framework of the EUROfusion Consortium, funded by the European Union via the Euratom Research and Training Programme (Grant Agreement No 101052200 — EUROfusion). Views and opinions expressed are however those of the author(s) only and do not necessarily reflect those of the European Union or the European Commission. Neither the European Union nor the European Commission can be held responsible for them.

This work has been carried out thanks to the support of the A*MIDEX project (n°ANR-11-IDEX-0001-02) funded by the “Investissements d’Avenir” French Government program, managed by the French National Research Agency (ANR).

References

[1] C. Bourdelle et al., WEST Physics Basis, Nuclear Fusion 55 (2015) 063017. https://doi.org/10.1088/0029-5515/55/6/063017

[2] J. Bucalossi et al., “Operating a full tungsten actively cooled tokamak: overview of WEST first phase of operation”, Nuclear Fusion 62 (2022) 042007. https://doi.org/10.1088/1741-4326/ac2525

[3] J. Gaspar et al., “Heat Flux estimation in WEST divertor with embedded thermocouples”, Journal of physics: Conference Series 745 (2016).

[4] Y. Corre et al., Review of Scientific Instruments 89, 063508 (2018) https://doi.org/10.1063/1.5024514
[5] N. Fedorczak et al., Infra-red thermography estimate of deposited heat load dynamics on the lower tungsten divertor of WEST, Physica Scripta, (2020), T171 https://doi.org/10.1088/1402-4896/ab4e3d
[6] R. Dejarnac et al., Flush-mounted Langmuir probes in the WEST tokamak divertor, Fusion Engineering and Design 163 (2021) 112120. https://doi.org/10.1016/j.fusengdes.2020.112120
[7] J. Gaspar et al., First heat flux estimation in the lower divertor of WEST with embedded thermal measurements, Fusion Engineering and Design 146 (2019) 757-760.
[8] J. Gaspar et al. "Divertor power loads and scrape off layer width in the large aspect ratio full tungsten tokamak WEST", Nuclear Fusion 61 (2021) 096027. https://doi.org/10.1088/1741-4326/ac1803
[9] M. Missirlian et al., "Manufacturing, testing and installation of the full tungsten actively cooled ITER-like divertor for WEST tokamak" this conference
[10] H. Roche et al., "HADES - High heAt loaD tESting - facility at CEA-IRFM", this conference
[11] J.P. Gunn et al., "Thermal loads in gaps between ITER divertor monoblocks: First lessons learnt from WEST", Nuclear Materials and Energy 27 (2021) 100920 https://doi.org/10.1016/j.nme.2021.100920
[12] J. Gaspar et al., "Surface heat flux estimation with embedded fiber Bragg gratings measurements: Numerical study" Nuclear Materials and Energy 12 (2017) 1077-1081 https://doi.org/10.1016/j.nme.2016.10.015
[13] Y. Corre et al., "First temperature database achieved with Fiber Bragg Grating sensors in uncooled plasma facing components of the WEST lower divertor" Fusion Engineering and Design 170 (2021) 112528 https://doi.org/10.1016/j.fusengdes.2021.112528
[14] J. Gaspar et al., "In-situ assessment of the emissivity of tungsten plasma facing components of the WEST tokamak", Nuclear Materials and Energy, 25 (2020) 100851. https://doi.org/10.1016/j.nme.2020.100851
[15] J. Gaspar et al., "Overview of the emissivity measurements performed in WEST: in-situ and post-mortem observations", Nuclear Fusion, accepted paper. https://doi.org/10.1088/1741-4326/ac6f68
[16] Garnier B et al., 2011 Measurements with contact in heat transfer: principles, implementation and pitfalls *Advanced School on Thermal Measurements and Inverse Techniques* (Roscoff)
[17] Verpaux P et al. CASTEM2000: a modern approach of computerised structural analysis 1988 Recent Advances in Design Procedures for High Temperature Plant
[18] K.O. Hill and G. Meltz., "Fiber Bragg Grating Technology Fundamentals and Overview" Journal of Lightwave Tehcnology, VOL. 15, NO. 8, August 1997
[19] G. Laffont et al., Meas. Sci. Technol. 24 (2013) 094010 (5pp)